Cluster Growth Model for Hydroxyapatite

Kazuo Onuma[†] and Atsuo Ito*[,‡]

National Institute for Advanced Interdisciplinary Research and National Institute of Materials and Chemical Research, 1-1-4 Higashi, Tsukuba, Ibaraki 305-8562, Japan, and National Institute for Advanced Interdisciplinary Research and Mechanical Engineering Laboratory, 1−1−4 Higashi, Tsukuba, Ibaraki 305-8562, Japan

Received February 3, 1998. Revised Manuscript Received August 31, 1998

An intensity-enhanced dynamic light scattering technique revealed the presence of calcium phosphate clusters from 0.7 to 1.0 nm in size in a simulated body fluid. The clusters were also present in fluids undersaturated with respect to octacalcium and amorphous calcium phosphates and supersaturated with respect only to hydroxyapatite. These clusters are the growth unit of hydroxyapatite judging from the fact that hydroxyapatite grows by step flow 0.8 or 1.6 nm in height and that the probability of incorporation of the growth unit into the crystal is extremely low, as revealed previously. We propose a cluster growth model where hydroxyapatite grows by selective hexagonal packing of left- and right-handed chiral $Ca_9(PO_4)_6$ clusters 0.8 nm in size. Theoretically, stacking faults of clusters create a reflection-twin crystal, edge dislocations with a Burgers vector of **C**/2 and screw dislocations. An example of the reflection-twin is the merohedry twin which is frequently found in cadmium chlorapatite. An atomic image corresponding to the edge dislocations with a Burgers vector of **C**/2 was actually obtained on the surface of synthetic single-crystal hydroxyapatite.

Introduction

Crystal growth of hydroxyapatite ($Ca_{10}(PO_4)_6(OH)_2$) makes an important contribution to ossification,[1,2] calculus formation,[3] arterial calcification,[4] and biomaterial performances.[5,6] A majority of information about crystal growth of hydroxyapatite has been obtained by the constant composition experiments using powdered hydroxyapatite as seeds. In a solution supersaturated as highly as a physiological solution, growth of hydroxyapatite is reported to proceed through the formation of a precursor with a Ca/P molar ratio of 1.45 ± 0.05 with the rate-determining process being a reaction at the surface.[7,8] In a less supersaturated solution, there is general agreement that the growth rates are too slow to be transport-controlled, although it is unclear which surface mechanism is rate-determining.[9,10] Both spiral growth and polynuclear models can explain the results of constant composition experiments and seeding experiments. Proposed rate-determining processes include dehydration of a calcium ion with diffusion jump,[9] migration of surface calcium and hydrogen phosphate groups,[10] and the building of hydroxyl ions.[11]

On the other hand, recent observations seem to require some new mechanism for hydroxyapatite crystal growth. An X-ray small angle scattering experiment or transmission electron microscopy suggest that growth proceeds with stacking of a unit as large as the size of unit cell of apatite (ca. 1 nm in size) in dental enamel and a biomimetic material.[12−14] Negatively charged substrates accelerated the nucleation and growth of hydroxyapatite compared with positively charged substrates.[15]

The ambiguity in the growth mechanism of hydroxyapatite arises from the difficulties in in situ observations of the growth process due to (a) limited availability of large single crystal seeds and (b) extremely slow growth rate. Nevertheless, in situ observation is the best way to investigate the essential growth mechanism. When powdered hydroxyapatite is used as seeds, measured growth rates are an average of the growth rate of each particle and in each crystallographical direction.

Using in situ atomic force microscopy (AFM) and a large hydroxyapatite single-crystal seed synthesized

* Corresponding author. TEL: +81-298-54-2557. FAX: +81-298-54-2565. E-mail: atsuoito@nair.go.jp.

[†] National Institute for Advanced Interdisciplinary Research and National Institute of Materials and Chemical Research.

[‡] National Institute for Advanced Interdisciplinary Research and Mechanical Engineering Laboratory.

(1) Palache, C.; Berman, H.; Frondel, C. *Dana's the System of mineralogy*, 7th ed.; John Wiley & Sons: New York, 1951; Vol. 2, p 887.

(2) Mann, S.; Webb, G.; Williams, R. J. P. *Biomineralization*; VCH Verlagsgesellschaft: Weinheim, 1989.

(3) Murphy, B. T.; Pyrah, L. N. *Br. J. Urol.* **1962**, *34*, 129.

(4) Doherty, T. M.; Detrano, R. C. *Calcif. Tissue Int.* **1994**, *54*, 224−230

(5) Schoen, F. J.; Harasaki, H.; Kim, K. M.; Anderson, H. C.; Levy, R. J. *J. Biomed. Mater. Res., Appl. Biomater.* **1988**, *22* A1, 11.

(6) Hench, L. L.; Wilson, J. *An Introduction to Bioceramics*; World Scientific: Singapore, 1993; p 8.

(7) Nancollas, G. H.; Mohan, M. S. *Archs Oral Biol.* **1970**, *15*, 731.

(8) Nancollas, G. H.; Tomazic, B. *J. Phys. Chem.* **1974**, *78*, 2218.

(9) Christoffersen, M. R.; Christoffersen, J. *J. Cryst. Growth* **1992**, *121*, 617.

(10) Nancollas, G. H.; LoRe, M.; Perez, L.; Richardson, C.; Zawacki, S. J. *Anatomical Record* **1989**, *224*, 234.

(11) Christoffersen, J.; Christofersen, M. R.; Johansen, T. *J. Cryst. Growth* **1996**, *163*, 304.

(12) Fratzl, P.; Fratzl-Zelman, N.; Klaushofer, K.; Vogl, G.; Koller, K. *Calcif. Tissue Int.* **1991**, *48*, 407.

(13) Miake, Y.; Shimoda, S.; Fukae, M.; Aoba, T. *Calcif. Tissue Int.* **1993**, *53*, 249.

(14) Walsh, D.; Hopwood, J. D.; Mann, S. *Science* **1994**, *264*, 1576.

(15) Yamashita, K.; Oikawa N.; Umegaki T. *Chem. Mater.* **1996**, *8*, 2697.

10.1021/cm980062c CCC: $15.00
Published on Web 10/20/1998

hydrothermally,[16] we succeeded in observing the growth process of hydroxyapatite in a simulated body fluid (2.5 mM $CaCl_2$, 1 mM $K_2HPO_4 \cdot 3H_2O$, 140 mM NaCl buffered at pH 7.4 by HCl and tris(hydroxymethyl)-aminomethane).[17,18] The growth on the *c*-face proceeded by a polynuclear mechanism.[19] The growth on *a*-face proceeded by step flow with step heights of 0.8 and 1.6 nm as well as by two-dimensional nucleation. Although these phenomena are qualitatively similar to those of other inorganic crystals, the step velocity on hydroxyapatite *a*-face showed two extraordinary features: (a) the step velocity was independent of the step height, and (b) step−step interaction was not observed even at interstep distances as low as 5 nm.[18] The former indicates that neither volume nor surface diffusion is the rate-determining process.[17] The latter means that the mean diffusion distance of an adsorbed growth unit is less than 2.5 nm on the surface. The mean diffusion distance should be 6.8−94 nm, i.e., a value 10−100 times longer than the lattice parameter of hydroxyapatite if dehydration of a growth unit entering the surface layer determines the growth rate.[20,21] Therefore, the dehydration process of a growth unit is not the rate-determining process. A remaining possibility for the rate-determining process was the incorporation process of a growth unit into bulk crystal. The step kinetic coefficient, β, the reciprocal of relative resistance of incorporation, was calculated to be 0.4×10^{-4} cm/s for the growth of the hydroxyapatite *a*-face.[18] This value was surprising because it was 100−1000 times lower than that of other inorganic crystals, being comparable to those of protein and virus crystals.[22,23] This means that the probability of incorporation of growth units into the bulk crystal is extremely low in the case of hydroxyapatite, which is similar to the case of protein crystals growing by the unit of a macromolecule having great anisotropy in shape and binding sites. Therefore, the growth unit of hydroxyapatite that determines the growth rate should not be simple spherical ions but should be some large cluster or ionic group with anisotropy that reduces incorporation probability. If the hydroxyapatite crystal grows by cluster units, some calcium phosphate cluster must be preformed in the solution. We report here the discovery of the presence of calcium phosphate clusters from 0.7 to 1.0 nm in size in a simulated body fluid found by an intensity-enhanced dynamic light scattering technique and propose a cluster growth model for hydroxyapatite.

Experimental Section

1. Dynamic Light Scattering. The theory of dynamic light scattering is as follows.[24] Fluctuation of light scattered by particles in a solution is analyzed by a photon correlation method under the concept of Rayleigh scattering. An autocorrelation function, $g(\tau)$, for photon count of scattered light is expressed as $g^2(\tau) = 1 + a|g^1(\tau)|^2$, where a is a constant, τ is a correlation time, $g^1(\tau)$ is the first-order correlation function, and $g^2(\tau)$ is the second-order correlation function. The $g^1(\tau)$ is related to the diffusion coefficient of particles, D, as $g^1(\tau) = \exp(-\Gamma\tau)$, $\Gamma = q^2D$, $q = 4\pi n/\lambda \sin(\theta/2)$, where Γ, n, λ, and θ are an attenuation constant, the refractive index of the solution, the wavelength of the light, and a scattered angle, respectively. From Stokes−Einstein's equation, the diameter of particles, d, is expressed as $d = kT/(3\pi\eta D)$, where k, T, and η are Boltzmann's constant, an absolute temperature, and the viscosity of the solution, respectively. Therefore, we can obtain the particle diameter, d, from the attenuation constant, Γ, of the autocorrelation function, $g^1(\tau)$.

When the particles have various sizes, $g^1(\tau)$ is expressed as a weighted sum of each $g^1(\tau)$ for the each particle size, where the weights should be calculated from a distribution function of Γ as a function of particle size. A histogram method uses values in a distribution histogram of finite numbers of Γ_i as weights instead of using the distribution function of Γ, and $g(\tau)$ is approximately expressed as $g^n(\tau) = \sum\Gamma_i \exp(-\Gamma_i\tau_i)$. Each Γ_i is calculated by a nonlinear least-squares method. The nonlinear least-squares method in the histogram method involves two different fitting analyses, i.e., a NNLS analysis and a Marquadt analysis. The former fits the data of $g(\tau)$ assuming that each kind of particle has no or little scatter in size. The size values can be calculated within a small deviation. However, the size values can be separated only when the size differences are more than twice or three times the particle size. On the other hand, the Marquadt analysis fits the data when assuming there is a scatter in the particle size.

A type DLS-7000 dynamic light scattering photometer (Ohtsuka Electric Co., Ltd.) was remodeled in three points to improve the detection limit of a particle size from its specification value of 3.0 nm down to less than 1.0 nm. First, a high-powered Ar ion laser (Spectra-Physics Co., Ltd.; multiline 4 and 1.2 W max. for 488 nm) was used to enhance the absolute scattered intensity. Second, an optically polished quartz cylindrical cell of 30 mm i.d. was used instead of a borosilicate glass cell of 15−20 mm i.d. to remove stray light from the cell wall, severely inhibiting stable measurement at a low scattering angle to detect subnanometer particles. Third, to remove dust, a pore size 40 nm filter was connected with a tube to the cell, and the filtration was performed using a peristaltic pump for 10 min at a flow rate of 15 mL/min without opening or removing the cell from the photometer. A simulated body fluid (2.5 mM $CaCl_2$, 1 mM $K_2HPO_4 \cdot 3H_2O$, 140 mM NaCl buffered at pH 7.4 by HCl and tris(hydroxymethyl)-aminomethane) without seed crystals was investigated under conditions of a 10° scattered angle, 256 channels, a 4 μs clock rate, and accumulation of 500 data acquisitions. Measured data were analyzed by the Marquadt method.

2. Atomic Force Microscopy (AFM). Lattice defects on an *a*-face of hydrothermally synthetic hydroxyapatite single crystals were observed by a type NanoScope III-a atomic force microscope (Digital Instruments) in the contact mode using a Si_3N_4 cantilever with a spring constant of 0.58 N/m.

Results

1. Particle Size Measurement for Reference Samples. For an accuracy check of the present dynamic light scattering system, molecular sizes of α-cyclodextrin and dehydrocholic acid sodium salt in solutions were measured as the size references. The former is toric in molecular shape in an aqueous solution and 1.46 × 0.8 nm in size.[25] The latter forms a stable dimmer of 1.2 nm in diameter (Murata, Y., personal

(16) Ito, A.; Nakamura, S.; Aoki, H.; Akao, M.; Teraoka, K.; Tsutsumi, S.; Onuma, K.; Tateishi, T. *J. Cryst. Growth* **1996**, *163*, 311.
(17) Onuma, K.; Ito, A.; Tateishi, T.; Kameyama, T. *J. Cryst. Growth* **1995**, *154*, 118.
(18) Onuma, K.; Ito, A.; Tateishi, T. *J. Cryst. Growth* **1996**, *167*, 773.
(19) Kanzaki, N.; Onuma, K.; Ito, A.; Teraoka, K.; Tateishi, T.; Tsutsumi, S. *J. Phys. Chem.* **1998**, *102*, 6471.
(20) Rosmalen, R. J.; Bennema P. *J. Cryst. Growth* **1975**, *29*, 342.
(21) Bennema, P.; Boon, J.; van Leeuwen, C.; Gilmer, G. H. *Kristall technik* **1973**, *8*, 659.
(22) Malkin, A. J.; Land, T. A.; Kuznetsov, Y. G.; McPherson, A.; DeYoreo, J. J. *Phys. Rev. Lett.* **1995**, *75*, 2778.
(23) Land, T. A.; Malkin, A. J.; Kuznetsov, Y. G.; McPherson, A.; DeYoreo, J. J. *Phys. Rev. Lett.* **1995**, *75*, 2774.
(24) Chu, B. *Laser Light Scattering*; Academic Press: New York, 1974.
(25) Fujiwara, R. *J. Cryst. Soc. Jpn*. **1982**, *24*, 54.

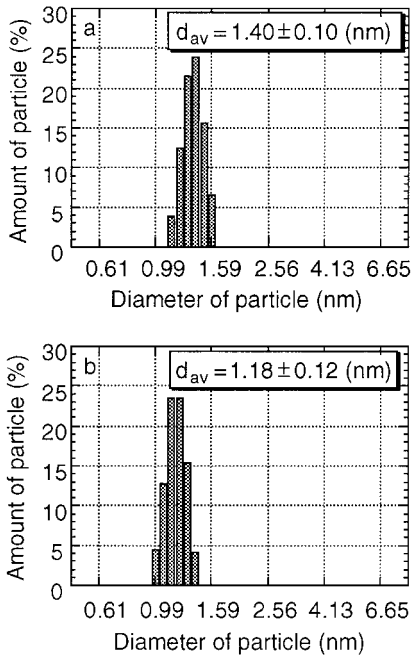

Figure 1. Particle size distributions for α-cyclodextrin (a) and dehydrocholic acid sodium salt (b) in solutions.

communication). The measured data are presented in Figure 1. The average sizes are found to be 1.40 ± 0.10 nm for α-cyclodextrin (Figure 1a) and 1.18 ± 0.12 nm for dehydrocholic acid sodium salt (Figure 1b), which shows good agreement with the reported values. Therefore, the present system is sufficiently accurate to measure particles at around 1 nm in size.

2. Particle Size Measurement for the Simulated Body Fluid. The raw data of the autocorrelation function for the simulated body fluid decreased quickly to 1.0 within 400 μs (Figure 2a). The size of particles in the fluid is from 0.4 to 1.0 nm with a peak at 0.7 nm, and a size fraction from 0.7 to 1.0 nm occupied 35−40% of total particles (Figure 2b). However, fluid containing only NaCl, tris(hydroxymethyl)aminomethane, and HCl, excluding calcium and phosphate ions, showed only a peak at 0.5 nm without having the fraction from 0.7 to 1.0 nm (Figure 2c). The peak at 0.5 nm corresponds to the size of a tris(hydroxymethyl)aminomethane molecule ($(CH_2OH)_3CNH_2$) because the sizes along the minor and major molecular axis of tris(hydroxymethyl)-aminomethane are calculated to be 0.49 and 0.62 nm, respectively, based on the atomic radii and bond length and angles for C, O, and N. Fluid containing NaCl, $K_2HPO_4 \cdot 3H_2O$, tris(hydroxymethyl)aminomethane, and HCl, excluding calcium ions, also showed a similar result, having a peak at 0.5 nm, although the size distribution becomes slightly wider (Figure 2d). Similarly, fluid containing NaCl, $CaCl_2$, tris(hydroxymethyl)-aminomethane, and HCl, excluding phosphate ions, showed a peak at 0.5 nm and no fraction from 0.7 to 1.0 nm (Figure 2e). Judging from these results, the size fraction from 0.7 to 1.0 nm observed in Figure 2b is ascribable to a calcium phosphate cluster. This fraction is not ascribable to a calcium phosphate complex,[26] $CaHPO_4^0$, because the size of the complex is estimated as 0.5−0.6 nm.

To confirm the presence of calcium phosphate clusters from strong solubility dependence of calcium phosphates upon pH of a solution, 1 N HCl was added to the simulated body fluid to decrease pH, and the change of the amount of clusters was monitored. The amount of 0.7−1.0 nm size fraction decreased with the decrease in pH and almost disappeared at least below pH 3.0 (Figure 2f). Values of ionic products at each pH value were calculated for hydroxyapatite and octacalcium and amorphous calcium phosphates as listed in Table 1 using the constants described elsewhere.[27] The simulated body fluid at pH 7.4 was found to be nearly saturated with respect to amorphous calcium phosphates and supersaturated with respect to octacalcium phosphate and hydroxyapatite. The simulated body fluid at pH 6.0 was supersaturated with respect only to hydroxyapatite. The simulated body fluid at pH 5.3 was nearly saturated with respect to hydroxyapatite. It is noted that the 0.7−1.0 nm size fraction still remains in the fluids at pH 6.0 and 5.3 (Figure 2f).

3. Surface Observation by AFM. An atomic image was obtained indicating the presence of many edge dislocations on the *a*-face of single-crystal hydroxyapatite (Figure 3). All the Burgers vectors of the dislocations were **C**/2, meaning that they were partial dislocations.

Discussion

The present dynamic light scattering study on the simulated body fluid demonstrated the presence of calcium phosphate clusters from 0.7 to 1.0 nm in size in the fluid. The simulated body fluid is a clear fluid. No spontaneous precipitation occurred from the fluid, even after the fluid had been kept at room temperature for, at least, 5 months. Nevertheless, the calcium phosphate clusters were present in the fluid. The clusters were present even when the fluid was undersaturated with respect to amorphous calcium and octacalcium phosphates and was supersaturated with respect only to hydroxyapatite. Theoretically, clusters with a size smaller than that of the critical nucleus can exist stably in solutions when a size-dependency of surface tension is taken into account in the theory of homogeneous nucleation.[34,35] Therefore, formation of calcium phosphate clusters does not necessarily mean the commencement of precipitation of amorphous calcium phosphate.

The involvement of "Posner cluster" ($Ca_9(PO_4)_6$) in the growth process of hydroxyapatite[36] is strongly suggested by the present findings as well as the previous results that hydroxyapatite *a*-face grows by step flow with a

(26) Vereecke, G.; Lemaître, J. *J. Cryst. Growth* **1990**, *104*, 820.
(27) Ito, A.; Maekawa, K.; Tsutsumi, S.; Ikazaki, F.; Tateishi, T. *J. Biomed. Mater. Res.* **1997**, *36*, 522.
(28) McDowell, H.; Gregory, T. M.; Brown, W. E. *J. Res. NBS-A Phys. Chem.* **1977**, *81A*, 273.
(29) Bell, L. C.; Mika, H.; Kruger, B. J. *Archs Oral Biol.* **1978**, *23*, 329.
(30) Moreno, E. C.; Brown W. E.; Osborn G. *Soil Sci. Soc. Proc.* **1960**, *24*, 99.
(31) Heughebaert, J. C.; Nancollas, G. H. *J. Chem. Eng. Data* **1985**, *30*, 279.
(32) Meyer, J. L.; Eanes, E. D. *Calcif. Tissue Res.* **1978**, *25*, 59.
(33) Christoffersen, M. R.; Christoffersen, J.; Kibalczyc, W. *J. Cryst. Growth* **1990**, *106*, 349.
(34) Larson, M. A.; Garside, J. *J. Cryst. Growth* **1986**, *76*, 88.
(35) Söhnel, O.; Garside, J *J. Cryst. Growth* **1988**, *89*, 202.
(36) Posner, A. S.; Betts, F. *Acc. Chem. Res.* **1975**, *8*, 273.

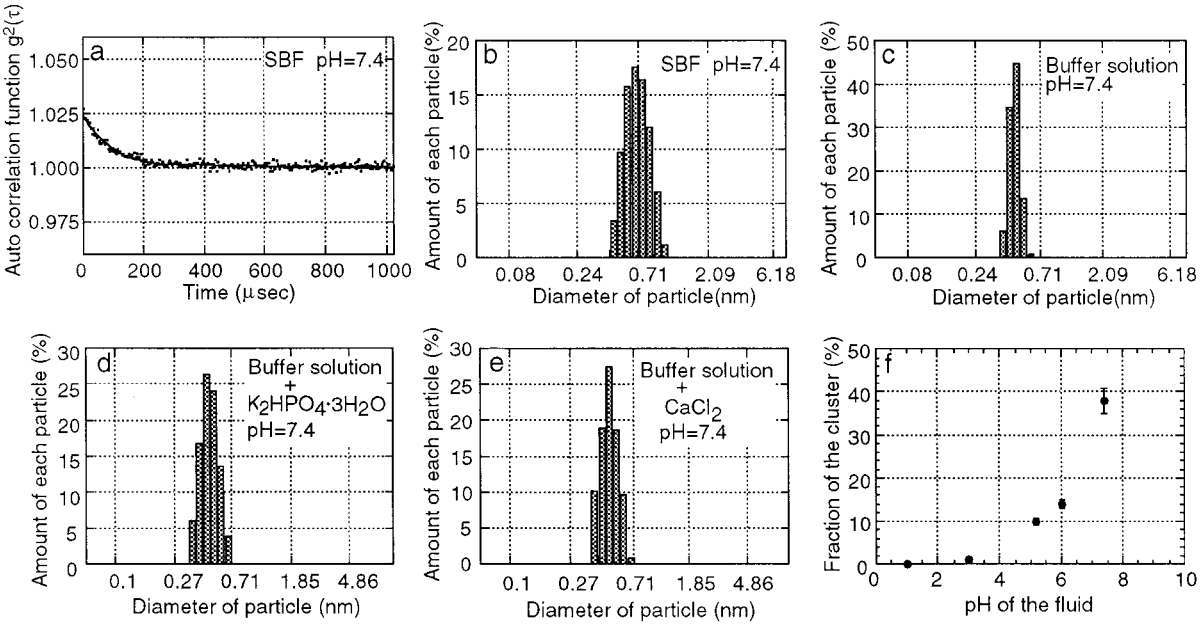

Figure 2. Autocorrelation function for the simulated body fluid (a). Particle size distribution in the simulated body fluid (b), in the fluid only containing NaCl, tris(hydroxymethyl)aminomethane, and HCl (c), in the fluid containing NaCl, $K_2HPO_4 \cdot 3H_2O$, tris(hydroxymethyl)aminomethane, and HCl (d), and in the fluid containing NaCl, $CaCl_2$, tris(hydroxymethyl)aminomethane, and HCl (e). The relation between the amount of calcium phosphate clusters, 0.7−1.0 nm in size, and the pH of the fluid (f).

Table 1. Ionic Activity Products for the Fluids for Hydroxyapatite and Octacalcium and Amorphous Calcium Phosphates at the pH Values Shown in Figure 2f

	negative logarithms of ionic activity products[b]		
phase[a]	pH 7.40	pH 6.00	pH 5.28
HAP	93.5 ± 0.2*[c]	109.3 ± 0.3*	119.0 ± 0.3
OCP	45.1 ± 0.1*	50.4 ± 0.1	53.8 ± 0.1†
ACP	25.7 ± 0.1	29.9 ± 0.1†	32.7 ± 0.1†
ACP1	10.9 ± 0.1	12.2 ± 0.1†	13.1 ± 0.1†

[a] HAP, OCP, and ACP denote hydroxyapatite, octacalcium phosphate, and amorphous calcium phosphate, respectively. [b] The ionic activity products are calculated following IPHAP = $(Ca)^{10}(PO_4)^6(OH)^2$, IPOCP = $(Ca)^4(H)(PO_4)^3$, IPACP = $(Ca)^3(PO_4)^{1.87}(PO_4)^{0.2}$, and IPACP1 = $(Ca)(PO_4)^{0.74}(H)^{0.22}$. The negative logarithms of solubility products for HAP, OCP, ACP and ACP1 are 115.0−118.7,[27−29] 46.9−49.6,[30,31] 24.8,[32] and 10.6.[33] respectively. [c] * and † indicate supersaturation and undersaturation, respectively, with respect to the corresponding phases.

height of 0.8 or 1.6 nm[17] and that the incorporation probability of a growth unit is extremely low.[17,18] We propose a following cluster growth model. The size of "Posner cluster" is 0.815 and 0.87 nm in the *a*- and *c*-directions, respectively, being consistent with the step height[17] and the cluster size found in the present study (Figure 4). It is pointed out first that the hydroxyapatite structure contains two distinct $Ca_9(PO_4)_6$ cluster units with different chirality: one is that centering on the Ca(1) site at the $z = 0$ level, namely C_0, while the other is that centering on the Ca(1) site at the $z = {}^1/_2$ level, namely C_{50}, sharing half of their volume in each other (Figure 4). They have a noncentrosymmetric C_3 symmetry resulting from a 3-fold rotation axis parallel to the *c*-axis and are mirror images with respect to the mirror planes at $z = {}^1/_4$ and ${}^3/_4$. Therefore, they are right- and left-handed chiral clusters and never superimpose each other. Statistical deficiency in calcium never affects the chirality of clusters because the chirality arises from phosphate arrangements as well. Bonding between clusters could be firmer in the *c*-direction than in the *a*-direction because the clusters interlock in the *c*-direction using two O(3) triangles with different sizes and orientations being present on the top and bottom of the cluster (Figure 4b).

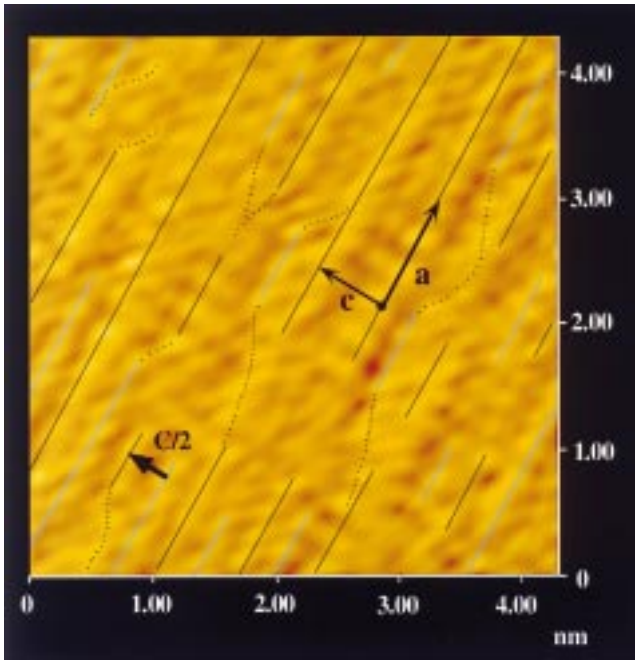

Figure 3. Atomic image of the *a*-face of hydroxyapatite crystal indicating the presence of partial dislocations with a Burgers vector of **C**/2 (arrow).

Hexagonal packing of the clusters automatically leads to a framework of a hydroxyapatite structure (Figure 5) whether the clusters have the stoichiometric composition or a slight calcium deficiency. However, to grow hydroxyapatite, the clusters must be arranged in either of two ways: one is that clusters of one of C_0 and C_{50} types are selectively arranged forming two-dimensionally a closed packing layer that is stacked, forming a-

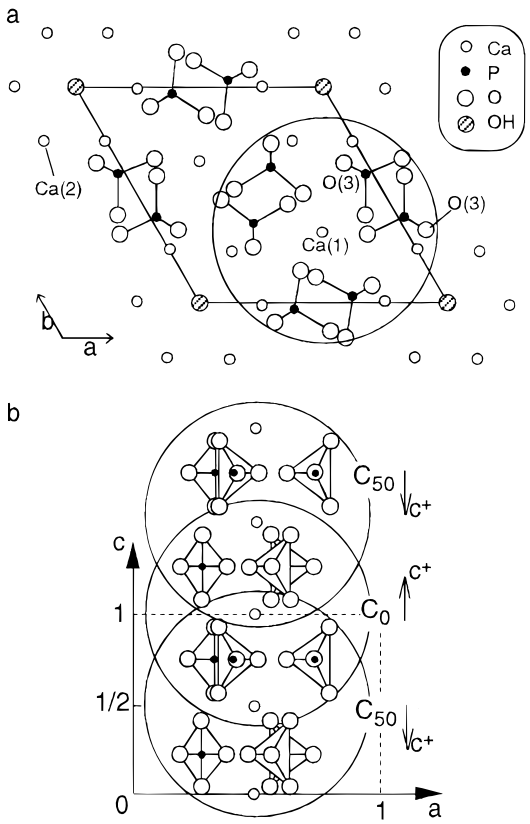

Figure 4. $Ca_9(PO_4)_6$ cluster units, C_0 and C_{50}, projected on the *ab* plane (a) and *ac* plane (b) of the hydroxyapatite structure. Because both cluster units have only C_3 symmetry (noncentrosymmetric) and are related by mirror planes at $z = 1/4$ and $3/4$, they are chiral.

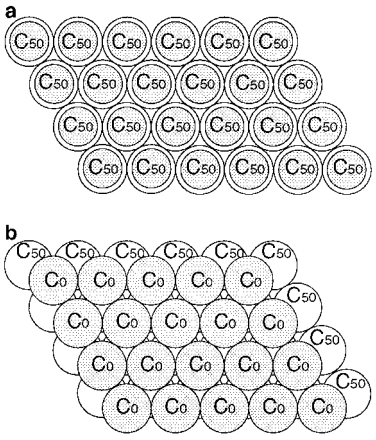

Figure 5. Two distinct packing of clusters to form hydroxyapatite structure. Open and dotted circles correspond to the first and second layer of stacking, respectively. (a) Hexagonal packing of either C_0 or C_{50} type clusters forming a primitive lattice. (b) Hexagonal closed packing with C_0 and C_{50} layers stacking alternatively.

hexagonal primitive lattice (Figure 5a); and the other is that the two-dimensionally closed packing layers of C_0 and C_{50} are stacked alternately, forming hexagonal closed packing (Figure 5b). In both cases, a process of chirality selection is required to grow hydroxyapatite.

The rest of the atoms, two OH groups and one Ca(1), are incorporated in the voids among the clusters. The OH groups and the Ca(1) atom have pyramidal and triangular coordination with three clusters, respectively, in the actual structure. The average radial ratio of OH ($r = 0.14$ nm) and Ca ($r = 0.099$ nm) to the cluster ($r = 0.4212$ nm) is 0.3323 and 0.235, respectively. These values closely coincide to the theoretical radial ratio for pyramidal coordination (0.414−0.225) and triangular coordination (0.225−0.155) for ions, respectively. Therefore, the cluster growth model is adequate from the viewpoint of crystal chemistry.

Table 2. The Types of Stacking Faults of Clusters

type[a]	clusters involved in the domains	orientation of the clusters	orientation of the interface vs the *c*-axis	results
1	C_0 & C_{50}	parallel	parallel	a reflection twin
2	C_0 & C_{50}	parallel	perpendicular	
3	C_0 & C_{50}	antiparallel	perpendicular	an edge dislocation
4	C_0 & C_{50}	antiparallel	parallel	a screw dislocation
5	(C_0 & C_0) or (C_{50} & C_{50})	antiparallel	parallel	a reflection twin
6	(C_0 & C_0) or (C_{50} & C_{50})	antiparallel	perpendicular	

[a] Stacking faults are expressed based on the hexagonal primitive lattice stacking (Figure 5a). The final results are unchanged when expressed as hexagonal closed packing as well (Figure 5b).

The rate-determining process proposed previously can be interpreted by the cluster growth model. It was proposed that the rate-determining process of hydroxyapatite growing under a condition similar to that in the present study was the conversion of the amorphous $Ca_3(PO_4)_2$ phase into hydroxyapatite, which occurred on the surface of hydroxyapatite seeds.[7,8] It was also reported that the conversion could involve an epitaxial matching between the depositing phase and hydroxyapatite substrate.[8] From the viewpoint of the present cluster growth model, the conversion with epitaxial matching means a process of rearrangement of stacked $Ca_3(PO_4)_2$ clusters and incorporation or migration of OH groups and Ca(1) into the voids among the clusters. Incorporation of OH groups was also proposed as the rate-determining process.[11] However, another possibility arises as the rate-determining process: chirality selection and orientation arrangement of clusters when the clusters incorporate into the hydroxyapatite lattice.

Stacking faults of the clusters to form domains having different cluster types or orientation result in a twin crystal or the creation of dislocations. There are six types of stacking faults depending on whether the cluster types involved are heterogeneous or homogeneous, whether the c^+ directions (Figure 4b) of two domains are parallel or antiparallel, and whether the interface between the domains is perpendicular or parallel to the *c*-axis (Table 2). Any stacking fault belongs to one of these six types or their combination. The type 1 and 5 stacking faults result in a reflection twin crystal with twin mirror planes parallel to the *c*-axis. An example of this kind of twin is the merohedry twin. The merohedry twin is frequently found in cadmium chlorapatite ($Cd_6(PO_4)_6Cl_2$), corresponding to the type 5 stacking fault.[37] The type 3 and 4 stacking faults result in a discrepancy by $1/2$ in *z* coordinates for all the atoms in one domain with respect to those in

(37) Donnay, J. D. H.; Sudarsanan, K.; Young, R. A. *Acta Crystallgr.* **1973**, *B29*, 814.

the other domain. Therefore, an edge dislocation with a Burgers vector of **C**/2 is formed when the domain interface is perpendicular to the *c*-axis (type 3). An atomic image corresponding to the edge dislocation with a Burgers vector of **C**/2 was actually obtained on the surface of single crystal hydroxyapatite grown hydrothermally (Figure 3). In the type 4 stacking fault, screw dislocations are formed when a transition zone is present at the interface (Figure 6). Therefore, the cluster growth model well explains the formation of twin crystals and dislocations.

The spiral growth mechanism of hydroxyapatite has not been established yet by direct evidences. Direct evidence has only established the contribution of spiral dislocations to the dissolution of apatite.[38,39] It is noted that the spiral dislocations can be introduced by the stacking fault of clusters even when hydroxyapatite does not grow by the spiral growth mechanism.

Finally, the $Ca_9(PO_4)_6$ cluster exists in the structure of octacalcium phosphate and amorphous calcium phosphate, both of which are the precursors of hydroxyapatite.[35,40] Therefore, the $Ca_9(PO_4)_6$ cluster could be an ultimate growth unit of hydroxyapatite, and correct arrangement of the $Ca_9(PO_4)_6$ clusters could mean the growth of hydroxyapatite. The following things remain to be clarified: the real chemical composition and concentration of the cluster in the fluid, whether the cluster mechanism is involved in heterogeneous nucleation processes, and whether the present growth model is applicable to an in vivo situation or in the presence of proteins and polysugars.

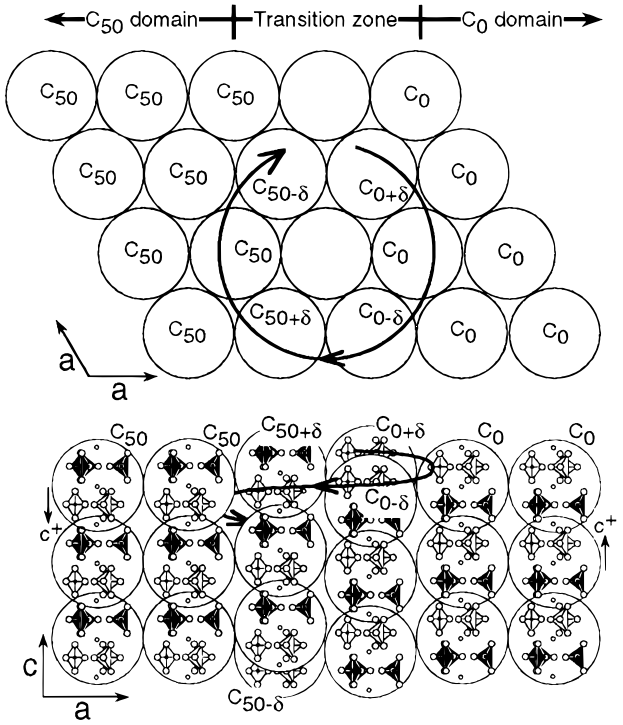

Figure 6. A screw dislocation formed by the type 4 stacking fault. In the transition zone, clusters slightly shift either upward or downward along the *c*-direction. The positional shift in *z* coordinate, δ, is expressed as $\delta = 100R/3T$, where R and T are the cluster diameter in *ab* plane and the width of transition zone, respectively. The figure represents the minimum width of transition zone ($T = 2R$).

Acknowledgment. This study was supported by AIST (Agency of Industrial Science and Technology). The authors would like to thank K. Teraoka for preparing hydroxyapatite single crystals and I. Tabe for preparing the figures.

CM980062C

(38) Jongebloed, W. L.; van den Berg, P. J.; Arends, J. *Calcif. Tissue Res.* **1974**, *15*, 1.
(39) Jongebloed, W. L.; Molenaar, I.; Arends, J. *Caries Res.* **1973**, *7*, 154.
(40) Brown, W. E.; Smith, J. P.; Lehr, J. R.; Frazier, A. W. *Nature* **1962**, *196*, 1048.